Supporting Information

Role of hyper-reduced states in hydrogen evolution reaction at sulfur vacancy in MoS_2

Kye Yeop Kim‡[1,2], *Joohee Lee*‡[1], *Sungwoo Kang*[1], *Young-Woo Son*[3], *Ho Won Jang*[1], *Youngho Kang*[*,4] & *Seungwu Han*[*,1,3]

[1]Department of Materials Science and Engineering and Research Institute of Advanced Materials, Seoul National University, Seoul 08826, Korea

[2]LG Electronics Yangjae R&D campus, 38, Baumoe-ro, Seocho-gu, Seoul 06763, Korea

[3]Korea Institute for Advanced Study, Seoul 02792, Korea

[4]Materials Modeling and Characterization Department, Korea Institute of Materials Science, Changwon 51508, Korea

‡ These authors contributed equally to this work.

Detailed electronic and structural character of *V*S and its concentration dependence

We first explain the structural distortion and electronic properties at low vacancy densities. Once a sulfur vacancy is created, neighboring ions around the vacancy site are relaxed. The largest relaxation occurs with the three nearest Mo ions that displace inward by 0.04 Å at 2.8% of the vacancy concentration. The vacancy defect in this concentration can be regarded as an isolated one because further decrease of the concentration does not influence the defect property. S-vacancy affects electronic property of MoS_2 by creating defect states inside the band gap which primarily derive from *d* states of neighboring Mo ions. There are three defect states labeled as a singlet a_1 and doubly degenerate *e* states based on the group theory. The a_1 state is fully filled by electrons in the neutral state, while the *e* states remain empty and are able to accept up to four excess electrons. These e states serve as the localization center for electrons, enabling the formation of hyper-reduced states.

In higher amount of vacancies, the structural distortion remains to be similar to that for the isolated vacancy detailed in the above. For example, the neighboring Mo ions are displaced inward by only 0.03 Å even at the largest defect concentration in the present study (~25%). About the electronic structure, more defect levels are introduced in higher vacancy concentrations (see Figure S1 below; the a_1- and *e*-derived states are marked in the green and red circles, respectively). These levels are still contributed by Mo ions neighboring the vacancy sites (see partial charge densities below). Since the electronic structure is essentially identical regardless of the vacancy density, we expect that the hyper-reduced state will also play an important role in the catalytic reaction at high vacancy concentrations, but the detailed thermodynamic and kinetic parameters could be different.

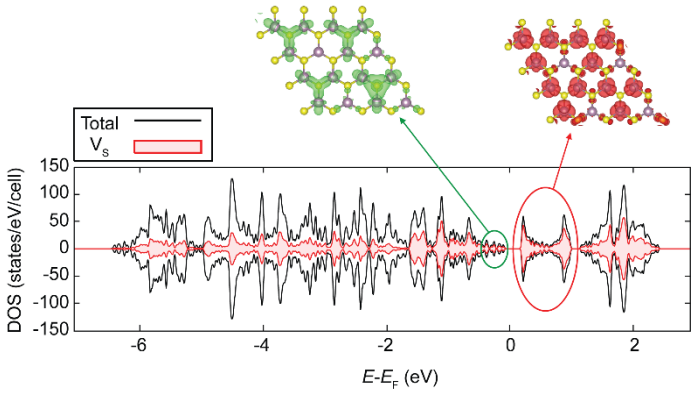

Figure S1. The density of states (DOS) of vacant MoS_2 with 25% of the S-vacancy concentration in the upper S plane. The a_1 related states are shown in green circle and e states in red circle. The corresponding partial charge density is also provided.

Free energy calculation

The free energy $G(n, q, N_{\mathrm{H}_2})$ of the system in Figure 1b where N_{H_2} molecules of H_2 evolved and the defect site is bonded to n hydrogen atoms ($0 \leq n \leq 2$) and charged with q, can be written as follows:

$$G(n, q, N_{\mathrm{H}_2}) - G(0,0,0) = G([n\mathrm{H} - V_{\mathrm{s}}]^q) + N_{\mathrm{H}_2}\mu_{\mathrm{H}_2}$$

$$-G([V_{\mathrm{s}}]^0) - (n + 2N_{\mathrm{H}_2} - q)\mu_e - (n + 2N_{\mathrm{H}_2})\mu_{\mathrm{H}^+} \quad , \qquad (1)$$

where $G(0,0,0)$ is the reference state. In eq 1, $(n + 2N_{\mathrm{H}_2} - q)$ and $(n + 2N_{\mathrm{H}_2})$ are differences in the electron and proton number with respect to the reference state, respectively. The eq 1 can be simplified by applying following equations:

$$\mu_e^{\mathrm{SHE}} + \mu_{\mathrm{H}^+} = \mu_{\mathrm{H}_2}, \qquad (2)$$

$$\mu_e = \mu_e^{\mathrm{SHE}} + eU, \qquad (3)$$

where e is the electron charge (< 0). The eq 2 corresponds to the SHE condition, assuming that the proton source of the reaction is only hydronium ions. The eq 3 represents the chemical potential of electron under the overpotential U applied to the cathode. In the SHE condition, $\mu_e^{\mathrm{SHE}} = -4.44$ eV. By removing μ_{H_2} and μ_{H^+} in eq. 1 using eqs 2 and 3, one obtains the following equation:

$$G(n, q, N_{\mathrm{H}_2}) - G(0,0,0) = G([n\mathrm{H} - V_{\mathrm{s}}]^q) - G([V_{\mathrm{s}}]^0) + q\mu_e^{\mathrm{SHE}} - \frac{n}{2}\mu_{\mathrm{H}_2} - eU(n + 2N_{\mathrm{H}_2} - q) \quad (4).$$

Step		Reaction formula	ΔG (eV)
$[V_S]^q \rightarrow [V_S]^{q-1}$	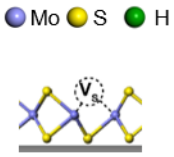	$[V_S]^{2+} + e^- \rightarrow [V_S]^+$	$-1.356+eU$
		$[V_S]^+ + e^- \rightarrow [V_S]$	$-1.219+eU$
		$[V_S] + e^- \rightarrow [V_S]^-$	$-0.049+eU$
		$[V_S]^- + e^- \rightarrow [V_S]^{2-}$	$0.286+eU$
		$[V_S]^{2-} + e^- \rightarrow [V_S]^{3-}$	$0.622+eU$
		$[V_S]^{3-} + e^- \rightarrow [V_S]^{4-}$	$0.780+eU$
$[\text{H-}V_S]^q \rightarrow [\text{H-}V_S]^{q-1}$	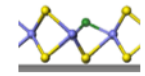	$[\text{H-}V_S]^+ + e^- \rightarrow [\text{H-}V_S]^0$	$-0.511+eU$
		$[\text{H-}V_S]^0 + e^- \rightarrow [\text{H-}V_S]^-$	$-0.185+eU$
		$[\text{H-}V_S]^- + e^- \rightarrow [\text{H-}V_S]^{2-}$	$0.381+eU$
		$[\text{H-}V_S]^{2-} + e^- \rightarrow [\text{H-}V_S]^{3-}$	$0.616+eU$
$[\text{2H-}V_S]^q \rightarrow [\text{2H-}V_S]^{q-1}$	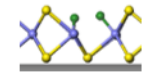	$[\text{2H-}V_S]^0 + e^- \rightarrow [\text{2H-}V_S]^-$	$-0.058+eU$
		$[\text{2H-}V_S]^- + e^- \rightarrow [\text{2H-}V_S]^{2-}$	$0.388+eU$

Table S1. The change in the Gibbs free energy during the charging step.

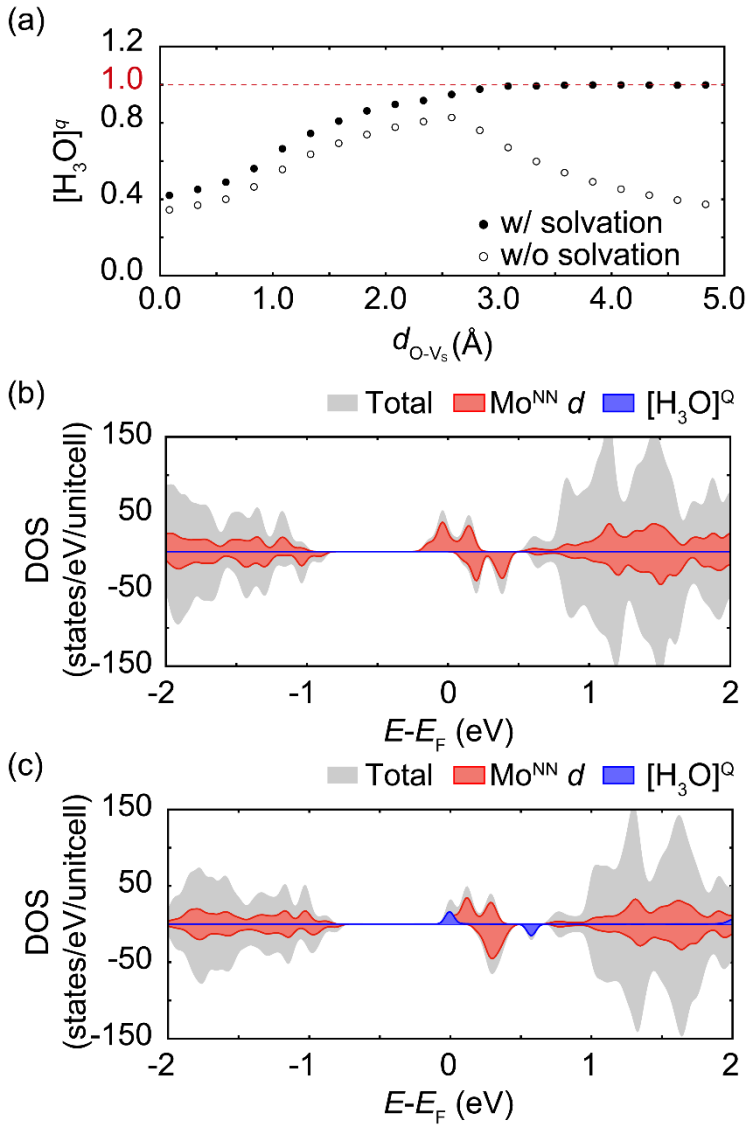

Figure S2. (a) Calculated charge q of a hydronium ion, $[H_3O^+]^q$, depending on the distance between $[H_3O]^q$ and V_S with or without solvation effects. The model system includes MoS_2 substrate with one V_S and one electron is removed from the neutral charge state of the whole system. It is seen that +1 charged state of $[H_3O^+]$ in water is properly described only when the solvation effects are included. (b), (c) Density of states (DOS) when the distance between $[H_3O^+]^q$ and V_S is 5 Å (b) with or (c) without solvation effects.

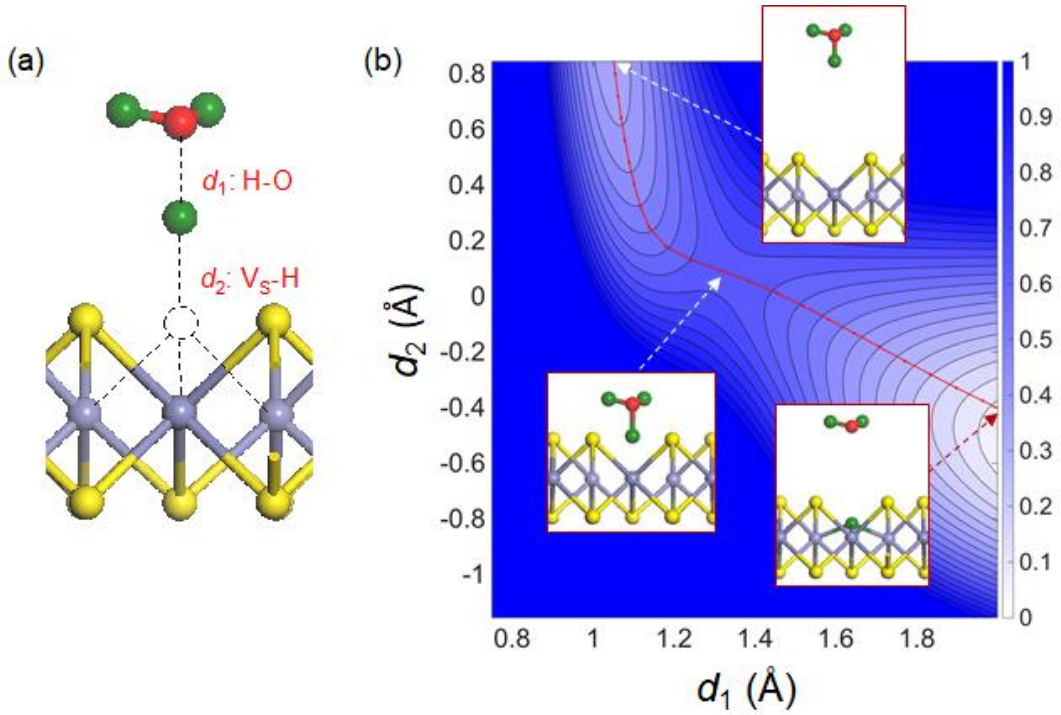

Figure S3. Since the NEB method in conjunction with solvation effects converge very slowly, we obtain the potential energy surface by the constrained minimization and identify the minimum energy path using the string method. (a) Constrained variables d_1 and d_2 in a Volmer step. (b) Potential energy surface of $[V_S]^- + H_3O^+ \longrightarrow [H\text{-}V_S]^0 + H_2O$ with respect to constrained variables of d_1 and d_2. The minimum energy path identified by the string method is noted as red lines. The initial, final, and transition states are shown as insets.

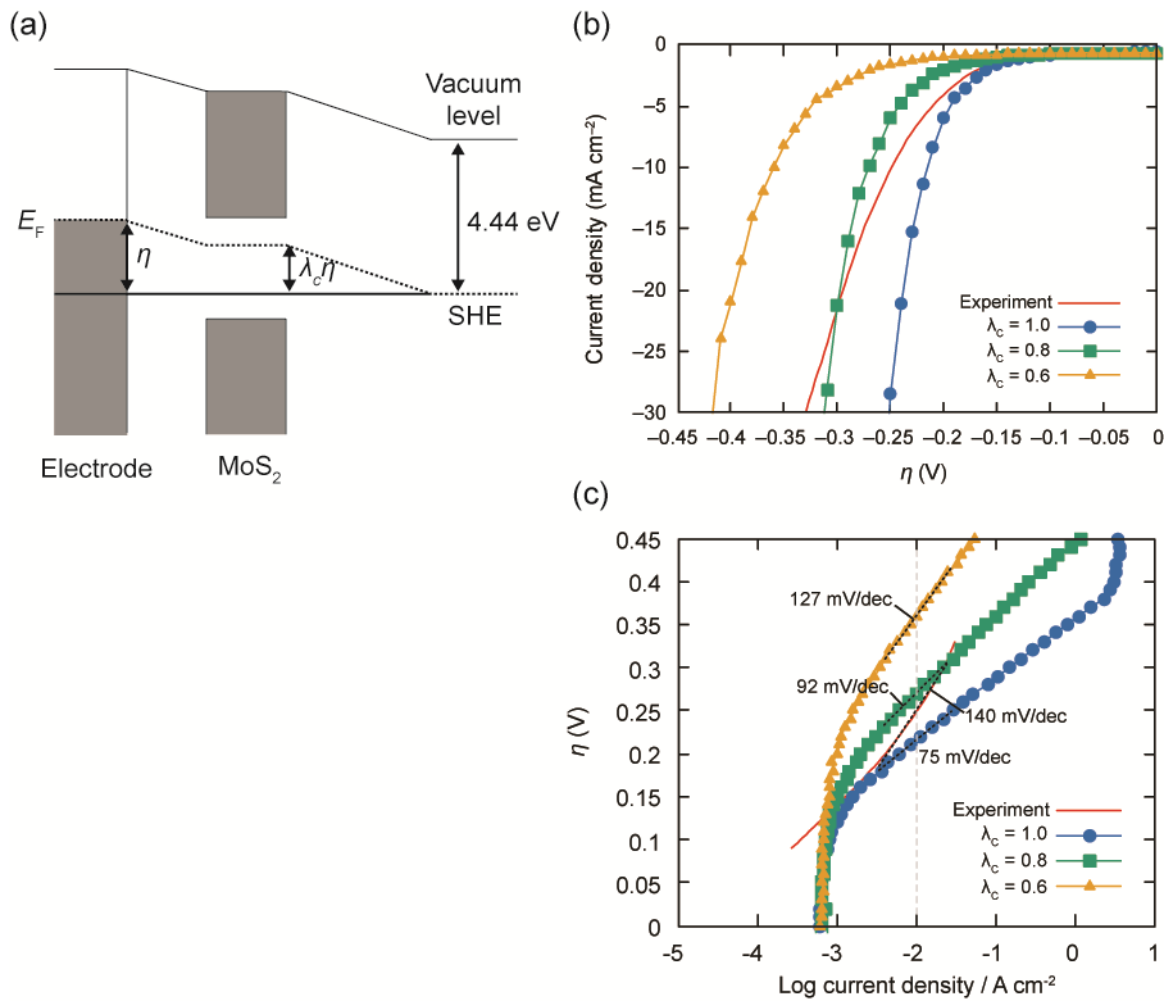

Figure S4. (a) Schematic diagram showing that the overpotential applied on MoS_2 (η_{MoS2}) is lower than for electrode (η) due to the bad contact. As a result, $\eta_{MoS2} = \lambda_c \cdot \eta$ ($\lambda_c \leq 1$) (b, c) Influence of λ_c on the (b) polarization curve, and (c) Tafel plot.

Table S2. ΔG and $\Delta G^{\ddagger}$ for elementary steps under the compressive strain of −1.35%.

Step		Reaction formula	ΔG (eV)	$\Delta G^{\ddagger}$ (eV)
Volmer	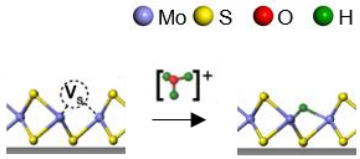	$[V_S] + H^+ \rightarrow [H\text{-}V_S]^+$	0.337	0.565
		$[V_S]^- + H^+ \rightarrow [H\text{-}V_S]^0$	−0.141	0.391
		$[V_S]^{2-} + H^+ \rightarrow [H\text{-}V_S]^-$	−0.649	0.191
		$[V_S]^{3-} + H^+ \rightarrow [H\text{-}V_S]^{2-}$	−0.947	0.086
		$[V_S]^{4-} + H^+ \rightarrow [H\text{-}V_S]^{3-}$	−1.106	0.000
	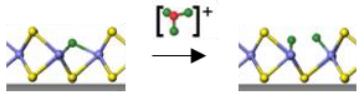	$[H\text{-}V_S]^- + H^+ \rightarrow [2H\text{-}V_S]^0$	0.420	1.028
		$[H\text{-}V_S]^{2-} + H^+ \rightarrow [2H\text{-}V_S]^-$	−0.021	0.694
		$[H\text{-}V_S]^{3-} + H^+ \rightarrow [2H\text{-}V_S]^{2-}$	−0.249	0.408
Heyrovsky	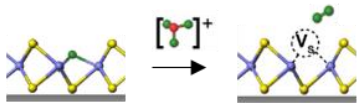	$[H\text{-}V_S]^+ + H^+ \rightarrow [V_S]^{2+} + H_2$	2.163	1.298
		$[H\text{-}V_S]^0 + H^+ \rightarrow [V_S]^+ + H_2$	1.195	0.921
		$[H\text{-}V_S]^- + H^+ \rightarrow [V_S]^0 + H_2$	0.036	0.971
		$[H\text{-}V_S]^{2-} + H^+ \rightarrow [V_S]^- + H_2$	−0.359	1.120
		$[H\text{-}V_S]^{3-} + H^+ \rightarrow [V_S]^{2-} + H_2$	−0.631	0.471
	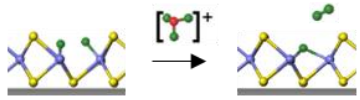	$[2H\text{-}V_S]^0 + H^+ \rightarrow [H\text{-}V_S]^+ + H_2$	−0.047	0.916
		$[2H\text{-}V_S]^- + H^+ \rightarrow [H\text{-}V_S]^0 + H_2$	−0.479	0.811
		$[2H\text{-}V_S]^{2-} + H^+ \rightarrow [H\text{-}V_S]^- + H_2$	−1.031	0.727
Tafel		$[2H\text{-}V_S]^0 \rightarrow [V_S]^0 + H_2$	−0.384	1.318
		$[2H\text{-}V_S]^- \rightarrow [V_S]^- + H_2$	−0.338	1.256
		$[2H\text{-}V_S]^{2-} \rightarrow [V_S]^{2-} + H_2$	−0.382	1.299
Charging	$[V_S]^q \rightarrow [V_S]^{q-1}$ 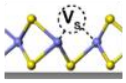	$[V_S]^{2+} + e^- \rightarrow [V_S]^+$	$-1.330+eU$	
		$[V_S]^+ + e^- \rightarrow [V_S]$	$-1.170+eU$	
		$[V_S] + e^- \rightarrow [V_S]^-$	$0.116+eU$	
		$[V_S]^- + e^- \rightarrow [V_S]^{2-}$	$0.497+eU$	
		$[V_S]^{2-} + e^- \rightarrow [V_S]^{3-}$	$0.809+eU$	
		$[V_S]^{3-} + e^- \rightarrow [V_S]^{4-}$	$0.928+eU$	
	$[H\text{-}V_S]^q \rightarrow [H\text{-}V_S]^{q-1}$ 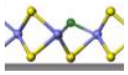	$[H\text{-}V_S]^+ + e^- \rightarrow [H\text{-}V_S]^0$	$-0.362+eU$	
		$[H\text{-}V_S]^0 + e^- \rightarrow [H\text{-}V_S]^-$	$-0.011+eU$	
		$[H\text{-}V_S]^- + e^- \rightarrow [H\text{-}V_S]^{2-}$	$0.511+eU$	
		$[H\text{-}V_S]^{2-} + e^- \rightarrow [H\text{-}V_S]^{3-}$	$0.769+eU$	
	$[2H\text{-}V_S]^q \rightarrow [2H\text{-}V_S]^{q-1}$ 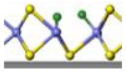	$[2H\text{-}V_S]^0 + e^- \rightarrow [2H\text{-}V_S]^-$	$0.070+eU$	
		$[2H\text{-}V_S]^- + e^- \rightarrow [2H\text{-}V_S]^{2-}$	$0.541+eU$	

Table S3. ΔG and $\Delta G^{\ddagger}$ for elementary steps under the tensile strain of 1.35%.

Step		Reaction formula	ΔG (eV)	$\Delta G^{\ddagger}$ (eV)
Volmer	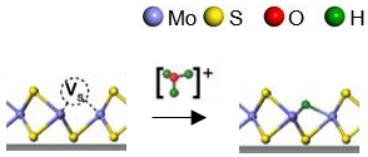	$[V_S] + H^+ \rightarrow [H\text{-}V_S]^+$	0.417	0.609
		$[V_S]^- + H^+ \rightarrow [H\text{-}V_S]^0$	0.014	0.485
		$[V_S]^{2-} + H^+ \rightarrow [H\text{-}V_S]^-$	−0.370	0.314
		$[V_S]^{3-} + H^+ \rightarrow [H\text{-}V_S]^{2-}$	−0.500	0.202
		$[V_S]^{4-} + H^+ \rightarrow [H\text{-}V_S]^{3-}$	−0.632	0.000
	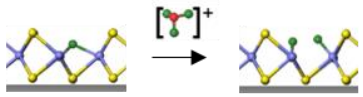	$[H\text{-}V_S]^- + H^+ \rightarrow [2H\text{-}V_S]^0$	0.408	1.024
		$[H\text{-}V_S]^{2-} + H^+ \rightarrow [2H\text{-}V_S]^-$	−0.007	0.644
		$[H\text{-}V_S]^{3-} + H^+ \rightarrow [2H\text{-}V_S]^{2-}$	−0.161	0.415
Heyrovsky	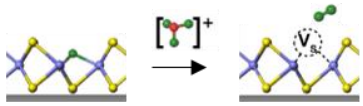	$[H\text{-}V_S]^+ + H^+ \rightarrow [V_S]^{2+} + H_2$	1.846	1.217
		$[H\text{-}V_S]^0 + H^+ \rightarrow [V_S]^+ + H_2$	1.290	1.027
		$[H\text{-}V_S]^- + H^+ \rightarrow [V_S]^0 + H_2$	0.619	0.902
		$[H\text{-}V_S]^{2-} + H^+ \rightarrow [V_S]^- + H_2$	0.279	0.695
		$[H\text{-}V_S]^{3-} + H^+ \rightarrow [V_S]^{2-} + H_2$	0.020	0.573
	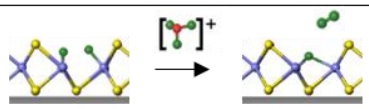	$[2H\text{-}V_S]^0 + H^+ \rightarrow [H\text{-}V_S]^+ + H_2$	0.628	0.904
		$[2H\text{-}V_S]^- + H^+ \rightarrow [H\text{-}V_S]^0 + H_2$	0.300	0.822
		$[2H\text{-}V_S]^{2-} + H^+ \rightarrow [H\text{-}V_S]^- + H_2$	−0.189	0.586
Tafel	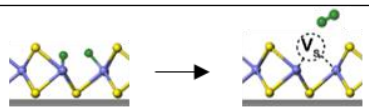	$[2H\text{-}V_S]^0 \rightarrow [V_S]^0 + H_2$	0.211	1.242
		$[2H\text{-}V_S]^- \rightarrow [V_S]^- + H_2$	0.286	1.206
		$[2H\text{-}V_S]^{2-} \rightarrow [V_S]^{2-} + H_2$	0.181	1.298
Charging	$[V_S]^q \rightarrow [V_S]^{q-1}$ 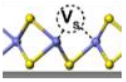	$[V_S]^{2+} + e^- \rightarrow [V_S]^+$	$-1.199+eU$	
		$[V_S]^+ + e^- \rightarrow [V_S]$	$-1.064+eU$	
		$[V_S] + e^- \rightarrow [V_S]^-$	$-0.240+eU$	
		$[V_S]^- + e^- \rightarrow [V_S]^{2-}$	$-0.009+eU$	
		$[V_S]^{2-} + e^- \rightarrow [V_S]^{3-}$	$0.230+eU$	
		$[V_S]^{3-} + e^- \rightarrow [V_S]^{4-}$	$0.382+eU$	
	$[H\text{-}V_S]^q \rightarrow [H\text{-}V_S]^{q-1}$ 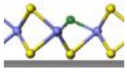	$[H\text{-}V_S]^+ + e^- \rightarrow [H\text{-}V_S]^0$	$-0.643+eU$	
		$[H\text{-}V_S]^0 + e^- \rightarrow [H\text{-}V_S]^-$	$-0.393+eU$	
		$[H\text{-}V_S]^- + e^- \rightarrow [H\text{-}V_S]^{2-}$	$0.100+eU$	
		$[H\text{-}V_S]^{2-} + e^- \rightarrow [H\text{-}V_S]^{3-}$	$0.250+eU$	
	$[2H\text{-}V_S]^q \rightarrow [2H\text{-}V_S]^{q-1}$ 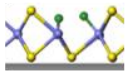	$[2H\text{-}V_S]^0 + e^- \rightarrow [2H\text{-}V_S]^-$	$-0.315+eU$	
		$[2H\text{-}V_S]^- + e^- \rightarrow [2H\text{-}V_S]^{2-}$	$0.096+eU$	

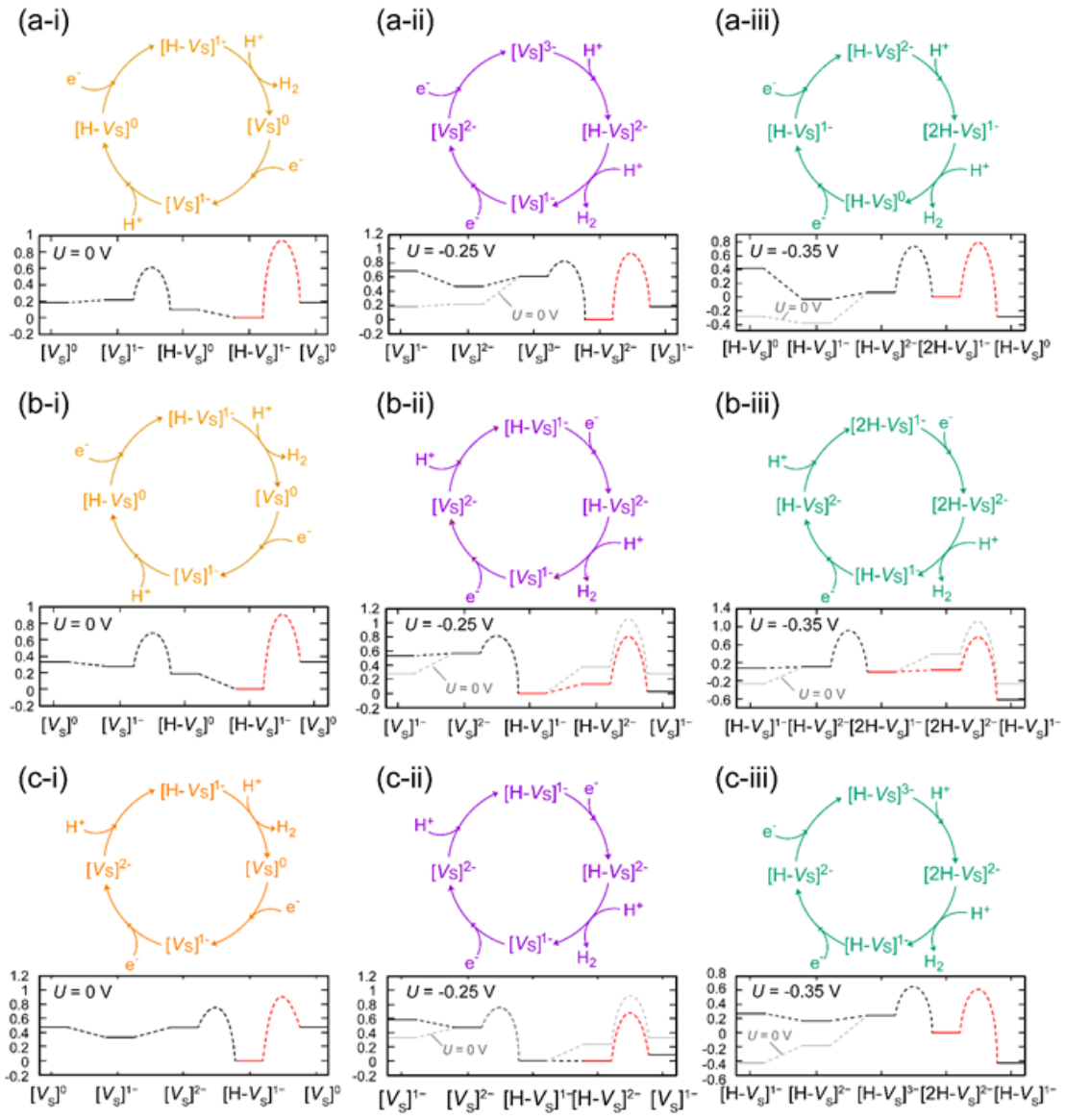

Figure S5. Major paths on different conditions of strain ((a) compressive, (b) no strain, and (c) tensile strain) when applied potential is i) 0, ii) −0.25, and iii) −0.35 V, respectively. The red line represents the rate-limiting step and gray lines represent the corresponding path when the potential is 0.

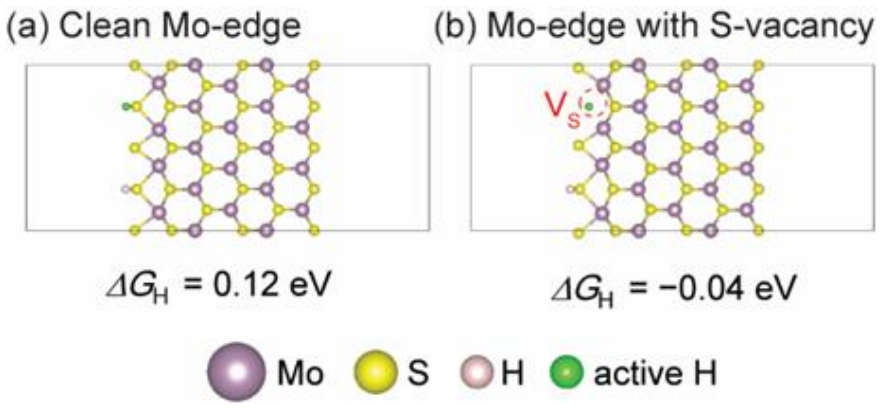

Figure S6. Mo-edge configurations (a) with and (b) without S-vacancy. We take into account the hydrogen coverage of 0.25 in one side of edges.

Table S4. The dependence of the hydrogen binding energy (ΔG_H) of V_S on the number of MoS_2 layers.

Number of layers	ΔG_H (eV)
1	0.02
2	0.03
3	0.03
4	0.03